Progress In Electromagnetics Research C, Vol. 172, 7–17, 2026

PIER C

(Received 2 May 2026, Accepted 8 June 2026, Scheduled 25 July 2026)

A Miniaturized 5.8 GHz WLAN Pentagonal Microstrip Antenna with Fractal DGS and FSS Reflector for Gain Enhancement

Nagari Naveen Kumar[1,2,*] and Dupakuntla Vishnu Vardhan[3]

[1]Department of ECE, Jawaharlal Nehru Technological University Anantapur, Ananthapuramu, A.P., India
[2]Department of ECE, J.N.T.U.A. College of Engineering (Autonomous), Ananthapuramu, A.P., India
[3]Department of ECE, J.N.T.U.A. College of Engineering (Autonomous), Pulivendula, A.P., India

ABSTRACT: In this article, a Miniaturized Pentagonal Antenna (MPA) with a Minkowski Curve, Fractal Defected Ground Structure (MCF-DGS), and Frequency Selective Surface (FSS) is proposed for 5.725–5.875 GHz WLAN application. The performance of a $\lambda/4$ transmission line-fed pentagonal patch antenna is examined using an iterated MCF-DGS etched on the ground plane. In the beginning, a fundamental antenna (Antenna-1) is designed and measured at 13.2 GHz with a S_{11} of -32.45 dB. After that, the resonant frequency of the fundamental MPA has been reduced from 13.2 GHz to 5.8 GHz by employing MCF-DGS (Antenna-2) with 56% miniaturization. The S_{11} of MCF-DGS measured for single-band frequency 5.8 GHz is -33.36 dB. The performance attributes of an MPA with improved efficiency, peak directivity, and peak gain via MCF-DGS and FSS (Antenna-3) are also analysed. The proposed antenna of $15 \times 16\,\text{mm}^2$ (or) $0.29\lambda_0 \times 0.30\lambda_0\,\text{mm}^2$ with a height of $h_1 = 1.6$ mm is designed, fabricated, and tested on a substrate of FR4 epoxy. The peak gain and peak directivity at 5.8 GHz are elevated from 1.74 to 7.40 dBi and 3.53 to 7.95 dBi by using an FSS composed of FR4, with a thickness of $h_2 = 1.6$ mm, situated under the MPA at a height of $h_3 = 8.5$ mm. The prototype model's test results are validated by the predicted outcomes of the proposed model.

1. INTRODUCTION

Antenna miniaturization has been the subject of studies for almost seven decades. Recently, numerous new studies have been performed to minimize the form factor (or overall dimensions) of various types of antennas while striving to preserve appropriate matching characteristics and operational bandwidth. These miniaturization strategies are typically associated with altering an antenna's electrical and physical characteristics. Fallahpours and Zoughi [1] posited that altered meandering lines, Koch-fragment tree, and designs influenced by materials and metamaterials are the primary methodologies for antenna miniaturization. The diminishment of antenna electrical size results in reduced bandwidth and efficiency, complicating matching due to the rise in antenna Q and spherical mode radiated fields referenced by Chu [2]. The notion of "an electrically small antenna" matches the reduction of antenna dimensions with Ka ≤ 1.0, whereas 'a' signifies a sphere radius that includes the antenna and K $= 2\pi/\lambda$ denotes the wave propagation vector [3]. Ziolkowski and Erentok [4] clarified the radiation properties that indicate a reduced bandwidth impedance, quality factor (Q), and peak gain for the development of compact antennas. Jahani et al. [5] examined resonators featuring an Mu-Negative (MNG) Metamaterial configuration for tiny antennas. Numerous miniaturization strategies have been devised for both non-planar slot and planar antennas, encompassing wires and loop methods [6–9]. Several antenna designs are employed in dimension-reduction techniques utilizing Fractals, Complimentary Split Ring Resonator (CSRR), Electromagnetic Band Gap (EBG), Single Split Ring Resonator (SSRR), and Split Ring Resonator (SRR) structures. Mishra ital. [13] examined a miniaturized antenna based on an electric LC resonator, characterized by good gain. DGS was employed to reduce patch dimensions and analyze collection elements [14–19]. Antennas engineered using multi-layer superstate designs exhibit enhanced peak directivity and peak gain [20, 21].

This study establishes two ways of miniaturization: one about antenna dimensions and the other treating the shifting of the resonant frequency. The Chu limit is attained by a miniaturized antenna, exhibiting size reduction. Changing the operating frequency is the idea behind using a smaller antenna with a 56% of resonant frequency miniaturization. The Chu limit was utilised to build an MPA, resulting in an increase in observed gain and directivity of MCF-DGS and FSS at 5.8 GHz, from 1.74 to 7.40 dBi and from 3.53 to 7.95 dBi, respectively, for WLAN applications. Table 1 shows that DGS-based antennas, in the literature, operating at lower frequencies generally have larger physical dimensions and lower peak gains than the proposed antenna.

2. MINIATURIZED ANTENNA DESIGN

The current investigation presents an MPA including Minkowski Curve, Fractal Defected Ground Structure (MCF-DGS) and Frequency Selective Surface (FSS), analyzed using ADS (Keysight Advanced Design System) and Ansys

* Corresponding author: Nagari Naveen Kumar (naveenecejntua@gmail.com).

TABLE 1. Comparison of recently reported DGS-based antenna miniaturization techniques with the proposed antenna.

Ref	size (mm^2)	Miniaturization (%)	Resonance shifting Frequency [GHz]		Working category	Gain (dBi) with respect to resonant frequencies	Methodologies
			Before shift	After shift			
[17]	$0.28\lambda * 0.28\lambda$	56.89	5.8	2.5	ISM	1.75	Rectangular slot with inner and outer of the concentric rings shaped
[18]	$0.2\lambda * 0.22\lambda$	47.36	5.7	3	WiMAX	8.9	Patch Antenna Array with power divider
[19]	$0.1\lambda * 1.25\lambda$	25.0	10	7.5	Arrays	4.12	Microstrip Patch Antenna with Spiral DGS
[20]	$1.149\lambda * 0.466\lambda$	57.77	5.8	2.45	ISM	2.14	Patch antenna with one cell and Two Cells of DGS
[21]	$0.125\lambda * 0.193\lambda$	53.6	5.8	2.69	Arrays	7.026	proposed antenna array 4×1
Proposed	$0.29\lambda * 0.30\lambda$	56	13.2	5.8	WLAN	6.70	KCF-DGS

TABLE 2. All optimal dimensions of the suggested antenna.

variables	Improved Value Measurement [mm]	variables	Improved Value measurement [mm]
Ground and substrate width, W_G and W_{Sub}	15	Length of feed, L_2	3.2
Ground and substrate length, L_G and L_{Sub}	16	Length of KCF-DGS covered was L_a	6.07
Patch pentagonal antenna with r_1	3	Length of Rectangular Slot, L_b	0.81
Width of feed, W_2	0.38	Length of Slot, L_c	1.7
Substrate thickness, h	1.6	Width of the Rectangular Slot, W_a	13.38
Feed Width, W_1 Length of feed L_1	2.3	Width of KCF-DGS, W_b	1.7

HFSS (High Frequency Structure Simulator). Figures 1(a) and 1(b) illustrate the upper and lower perspectives of the proposed MPA, which is energized by a 50 ohms connector and has an MCF-DGS created on the surface of the MPA's ground plane. Equations (1) and (2) denote the length of the feeder (L_f) and microstrip line impedance (Z_0), respectively [22]. The substrate, composed of FR4 and measuring 1.6 mm of thickness, exhibits a dielectric permittivity of 4.4 and dimensions of $0.29\lambda_0 * 0.3\lambda_0\,mm^2$. A pentagonal patch with a fillet radius of 0.3 mm is used to smooth the vertex edges of the pentagonal antenna, and $r1 = 3$ mm is utilized for WLAN application.

$$L_f = \frac{L_{\lambda/4}}{\pi}\cos^{-1}\sqrt{\frac{50}{z0}} \quad (1)$$

$$Z_0 = \frac{377}{\sqrt{\varepsilon_r\left(\frac{w}{h} + 1.393 + 0.667\ln\left(\frac{w_f}{h} + 1.444\right)\right)}} \quad (2)$$

2.1. Construction of Minkowski Curve, Fractal Defected Ground Structures

Table 2 presents improved values of the suggested antenna, and Figures 1(a)–(d) show the geometry of a pentagonal antenna using a Minkowski Curve, Fractal Defected Ground Structure (MCF-DGS) technique. The proposed antenna was miniaturized by 56%, which can switch between 13.2 and 5.8 GHz. The miniaturized pentagonal antenna with MCF-DGS proposed here is intended to proceed with the Chu limit [1] from the third equation. An antenna is encased within a sphere, represented by the letter 'a'.

$$Q_{chu} = \frac{1}{ka} + \frac{1}{(ka)^3} \quad (3)$$

In Chu et al. [2], a numerical correlation was suggested between the source dispersion and its association with the configuration of the antenna within the sphere. A sphere with a radius of 7.5 mm was used to calculate the Chu limit for a patch with a miniaturized antenna including the MCF-DGS. Koch curve

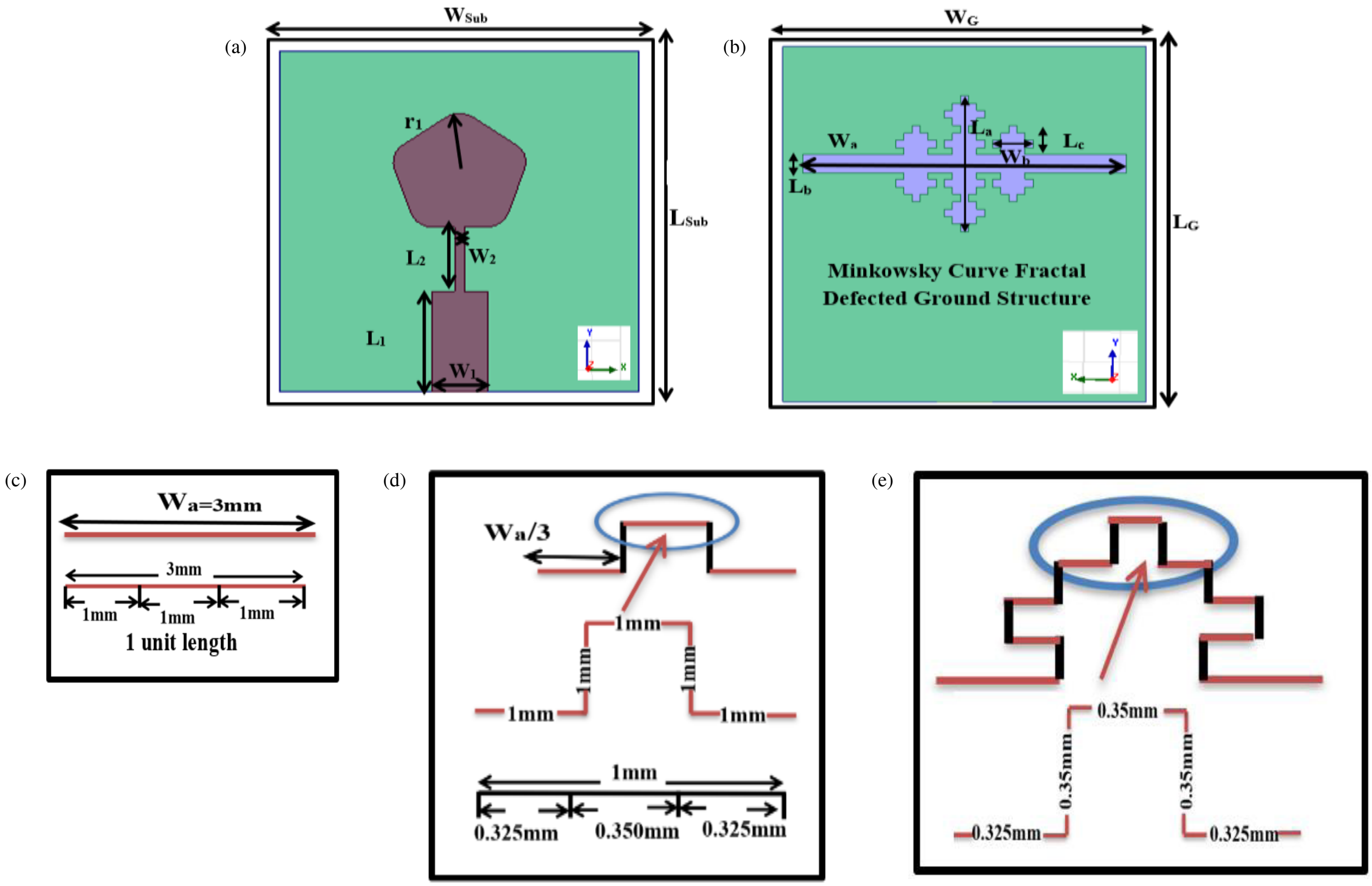

FIGURE 1. Miniaturized pentagonal antenna with an MCF-DGS geometry. (a) Upper view, (b) view from the bottom, (c) Minkowski curve, fractal defected ground structures: iteration zero, (d) iteration one, and (e) iteration two.

concept is used to design the proposed geometry at the periphery of the slot with dimensions of $3 \times 0.35\,\text{mm}^2$. An MCF is partitioned into n sections, where $W_{m1dgs} = L$ geometric sections. A technique for segmenting a line is illustrated in Figures 2(d)–(f). The same frameworks are employed for all iterations to substitute the central sections. Each repetition increased the line length to five-thirds of the original. According to Equation (4), the revised dimension is L_n.

$$L_n = L(5/3)^n \tag{4}$$

The length of the initial line is L, and the length of the subsequent line after n repetitions is L_n. The suggested antenna consists of two iterations, $n = 2$.

The design procedure is elaborated further below. Figure 2 illustrates the procedures undertaken to finalize the prototype of the single-band miniaturized Minkowski Curve, Fractal Defected Ground Structure (MCF-DGS). A pentagonal radiator functioning in the Ku-band at 13.2 GHz, exhibiting a gain of 6.49 dBi and bandwidth impedance of 6.049% is presented in the 1st case (Figure 2(a)). The proposed antenna was altered by removing the KCF defective structure from the ground plane. This etching was performed to reduce the frequency band. Consequently, the concept of antenna miniaturization involves transitioning the frequency from the Ku band (f_1) to the C band (f_2) without modifying the antenna size. Equation (5) represents the Miniaturization Factor [23, 24].

$$M = \frac{f_2}{f_1} \tag{5}$$

The implementation of a DGS with a microstrip antenna causes a disruption in current distribution owing to the carved flaw on the ground plane. The flow of surface current and characteristic impedance parameters are affected along the path of the antenna's capacitance and inductance values, which result from variations in current distribution [20]. The working frequency is altered from 13.2 to 5.8 GHz attributable to an augmentation in the path of electrical length (βl) of the proposed antenna. Following the implementation of the initial repetition of Koch Curve Fractal (KCF)-DGS on the ground-based bottom plane, the gain diminished to 1.79 dBi, and the bandwidth impedance contracted to 10.35% at the operational frequency of 5.87 GHz, as illustrated in instance 2 of Figure 2(b). Subsequently, the KCF-DGS, second iteration, is etched onto the substrate, leading to a decrement of 1.71 dBi in gain, a shift in resonant frequency to 5.84 GHz, and a bandwidth impedance of 5.88%, as illustrated in case-3 of Figure 2(c). Altering the proposed antenna design structure that supports the third iteration of KCF-DGS on the ground plane enables the antenna to function at a smaller frequency band, leading to a reduction in frequency. Case-4 in Figure 2(d) indicates that at 5.76 GHz,

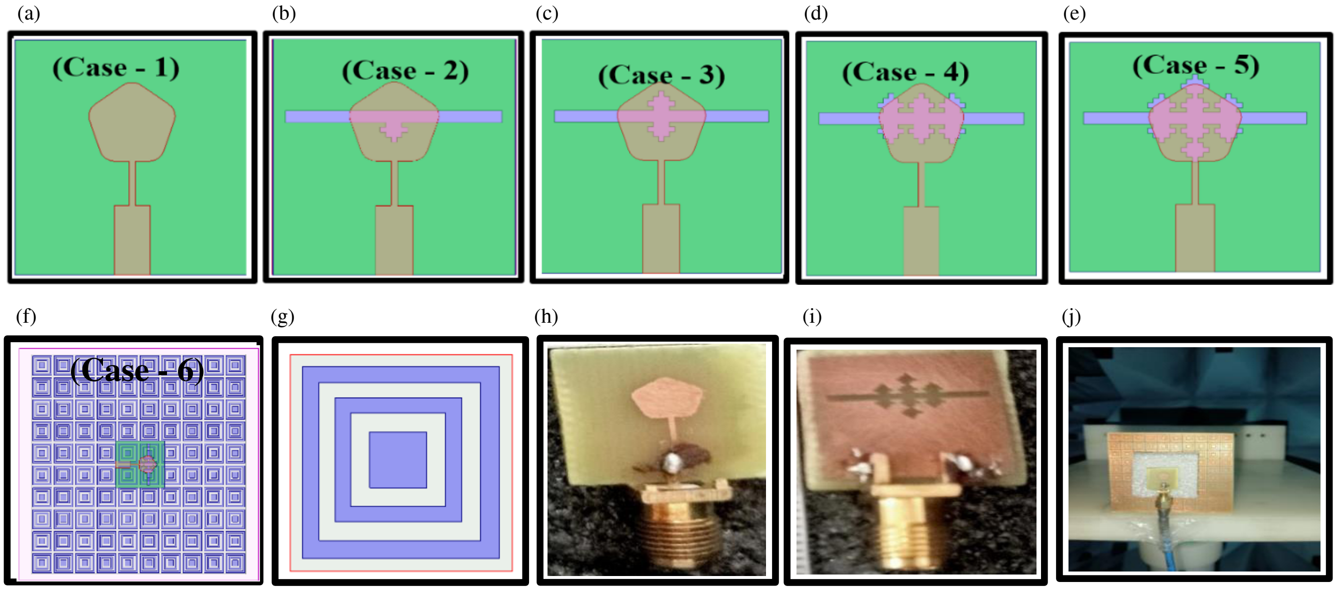

FIGURE 2. The procedures for developing a single-band miniaturized antenna: (a) quarter wave-fed traditional antenna, (b) 1st repetition, (c) 2nd repetition, (d) 3rd repetition of KCF-DGS, (e) KCF-DGS on the surface of ground view, (f) FSS positioned beneath the conventional antenna, (g) structure of FSS, (h) upper view, (i) reverse view, and (j) testing room of the constructed prototype.

TABLE 3. Attributes of miniaturized antennas for various phases.

parameter	Case-1	Case-2	Case-3	Case-4	Case-5	Case-6
Resonant freq. (GHz)	13,2	5.85	5.84	5.76	5.8	5.8
Ka and Q_{chu}	2.07, 0.59	0.91, 2.38	0.91, 2.39	0.90, 2.46	0.91, 2.42	0.91, 2.42
Gain (dBi)	6.49	1.79	1.71	1.81	1.74	7.40
Bandwidth (GHz)	0.80	0.61	0.62	0.58	0.64	0.72
Directivity (dBi)	7.59	3.71	3.51	3.45	3.53	7.95
Efficiency (%)	97.8	65.2	64.6	63.4	60.1	82.5
E-plane (dB) $\theta = 0°$, $\phi = 0°$	8.78	4.17	-12.30	0.945	6.19	5.78
H-plane (dB) $\theta = 90°$, $\phi = 90°$	-7.68	-5.12	-2.39	-2.43	-4.14	-5.18

the gain is enhanced to 1.81 dBi, accompanied by a bandwidth impedance of 10.06%. Using rectangular-slot geometry on the ground, current is disrupted throughout the patch, due to which the resonance frequency is shifted by increasing the electrical length (βl), which affects capacitance and inductance values, resulting in an increase in realized gain and a decrease in resonant frequency. As depicted in case-5 in Figure 2(e), the gain is 174 dBi at a frequency of 5.8 GHz. Finally, in case-6 of Figure 2(f), Miniaturized Pentagonal Antenna (MPA) with a Minkowski Curve, Fractal Defected Ground Structure (MCF-DGS) and Frequency Selective Surface (FSS) is suggested for 5.8 GHz WLAN application. The suggested patch antenna is manufactured after the simulation results have been verified. Photographs of the manufactured antenna, which measures $15 \times 16 \times 1.6\,\text{mm}^3$, with and without DGS and FSS, are shown in Figures 2(h)–(j). The MITS prototype machine is used to manufacture the suggested antenna with DGS and FSS, and the Vector MS2037C Network Analyser (VNA) is used for experimentation. The characteristics of the miniaturized antenna at different stages are compared in Table 3, from case-1 to case-6.

Figures 3(a) and 3(b) illustrate the layout model and lumped equivalent circuit of the proposed single-band antenna, respectively. An effective method for addressing this issue is to incorporate an integrated element in the equivalent schematic representation utilizing ADS for every component of the suggested schematic antenna. Correct modeling of the antenna is required to determine the correct values of elements. The subsequent values of L, R, and C correspond to the frequency of the patch antenna. The subsequent Equations (6)–(9) facilitate the calculation of similar circuit (L, C, and R) parameters and the assessment of the quality factor of the resonator. X denotes the feed point location.

$$C = \frac{\varepsilon_0 \varepsilon_r LW}{2h} \cos^2 \frac{\pi X_0}{L} \tag{6}$$

$$L = \frac{1}{C\omega_r^2} \tag{7}$$

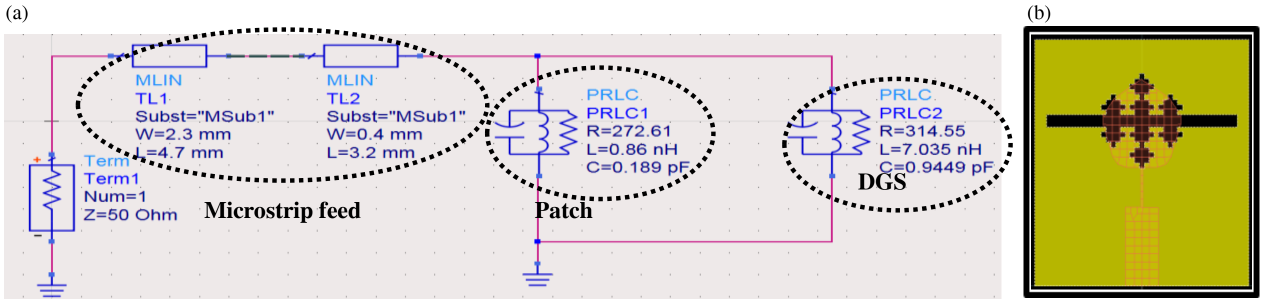

FIGURE 3. (a) Model of similar circuits and (b) layout for miniaturized patch antenna with KCF-DGS using ADS.

$$R = \frac{Q}{C\omega_r^2} \tag{8}$$

$$\text{Quality Factor, } Q = \frac{c\sqrt{\varepsilon_e}}{4fh} \tag{9}$$

The parameters L_F and C_F in the equivalent circuit of the line feed are defined by Eqs. (1) and (11), respectively

$$L_F = 100h\left(4\sqrt{\frac{w_f}{h-4.21}}\right)\text{ (nH)} \tag{10}$$

$$C_F = W_f[(9.5\varepsilon_r + 1.25)\frac{w_f}{h} + 5.2\varepsilon_r + 7]\text{ (pF)} \tag{11}$$

The adjusted values of parameters of the compared equivalent circuits are optimized parameter values extracted from the lumped equivalent circuit, which are $L_p = 0.86$ nH, $C_p = 0.189$ pF, $R_P = 272.61\,\Omega$ of the patch. $TL1$ consists of $w = 2.3$ mm, $L = 4.7$ mm, and $TL2$ consists of $w = 0.4$ mm, $L = 3.2$ mm. $R_{dgs} = 314.55$ ohms, $Ldgs = 7.035$ pH, and $Cdgs = 0.9449$ pF are calculated respectively as illustrated in Figure 3(a).

2.2. Principles of FSS Reflectors Employed to Enhance the Gain of the Proposed Antenna

Figure 4(a) shows the miniaturized antenna's side view with an FSS reflector. The compact single-layer miniaturized antenna with an FSS reflector developed in this investigation comprises two square-ring resonant components, as shown in Figure 4(b). The impedance bandwidth can be improved by increasing the electrical size of the complete reflector using the four branches of the two square rings. The thickness ($h2$) of the 1.6 mm FR4 epoxy substrate was used to create the FSS model. For FSS analysis, the equivalent circuit model (ECM) provides a quick and easy method. The fundamental unit form is a square loop, which is comparable to the LC series model [26]. Figure 4(c) illustrates the identical circuit model of the developed frequency selective surfaces (FSSs). The ECM's capacitance and inductance can be solved using Eqs. (12)–(16), where θ is the incidence angle, and D, P, S, and gap are the FSSs' square loop dimensions listed in Table 4. The corresponding circuit of the outer loop is depicted in Figure 4(c), where the space between the two adjacent parts provides capacitance $C1$, and the loop contributes to inductance $L1$. Similarly, the inductances $L2$ and $L3$ and capacitance $C2$ of the inner loop are known. According to Eqs. (11)–(16), $L1 = 10.97$ nH, $C1 = 0.0686$ pF, $L2 = 5.49$ nH, and $C2 = 0.0343$ pF, $L3 = 5.49$ nH. Figure 4(d) shows the entire top view of the miniaturized proposed antenna.

TABLE 4. FSS reflector unit cell dimensions (mm).

variable	D	gap	P	S
value	4	0.35	4.35	1

$$\frac{B_C}{Y_0} = \omega c = 4\frac{d}{p}sec\theta F(p,g,\lambda)\varepsilon_{\mathit{eff}} \tag{12}$$

$$\text{Where } F(p,s,\lambda) = p\lambda[\ln \mathrm{cosec}\pi s2p + G(p,s,\lambda)] \tag{13}$$

$$G(p,s,\lambda) = \frac{1}{2}\times \frac{(1-\beta^2)^2\left[\left(1-\frac{\beta^2}{4}\right)(A_+ + A_-) + 4\beta^2 A_+A_-\right]}{\left(1-\frac{\beta^2}{4}\right)+\beta^2\left(1+\frac{\beta^2}{2}-\frac{\beta^2}{8}\right)(A_+ + A_-)+2\beta^6 A_+A_-} \tag{14}$$

$$A_\pm = \frac{1}{\sqrt{1\pm\frac{2p\sin\theta}{\lambda}-\left(\frac{p\cos\theta}{\lambda}\right)^2}} - 1; \quad \beta = \sin\frac{\pi s}{2p} \tag{15}$$

$$\varepsilon_{\mathit{eff}} = \frac{\varepsilon_r+1}{2} - \frac{\varepsilon_r-1}{2}\times\exp\left(\frac{-13h}{p}\right) - \left(\frac{100s^2}{d} - 2g + 10h\right) \tag{16}$$

3. RESULTS AND DISCUSSION

The reaction of the circuit model was compared with the HFSS simulation response, as illustrated in Figure 5(a). This outcome indicates a strong concordance between these two graphs. Both answers exhibit an S_{11} of approximately -32.46 at the resonant frequency of 13.2 GHz. The measured and simulated return losses are displayed at 5.8 GHz, demonstrating strong concordance in Figure 5(b). The simulated S_{11} is pertinent to the development of a single-band miniaturized antenna, as shown in Figure 5(c). Figure 5(d) illustrates a simulation of KCF-DGS with (iteration 0) with a different slot size 'W_0'. Because of

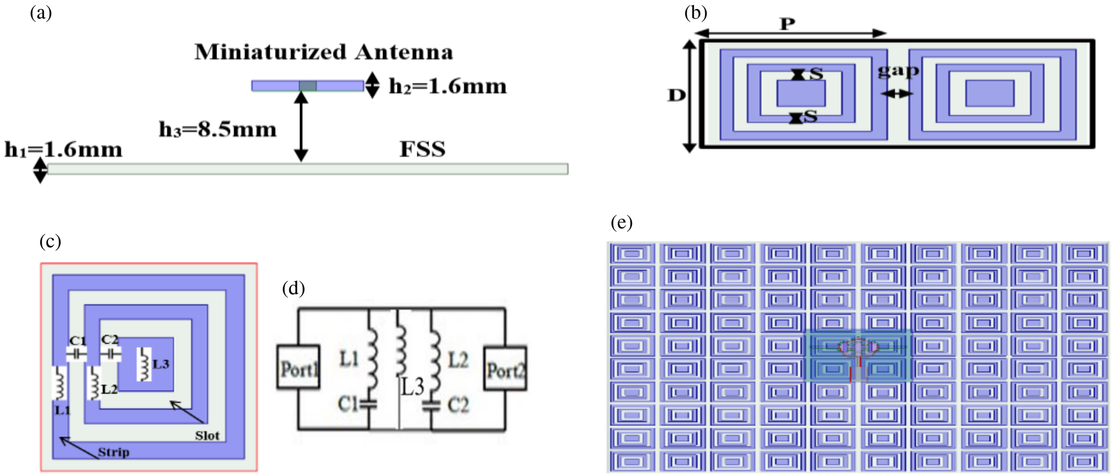

FIGURE 4. (a) Lateral view of the miniaturized antenna using DGS and FSS reflector, (b) FSS unit cell dimensions, (c) equivalent representation of FSS unit cell, (d) equivalent circuit of FSS, and (e) top view of the miniaturized antenna using DGS on the FSS reflector (Antenna-3).

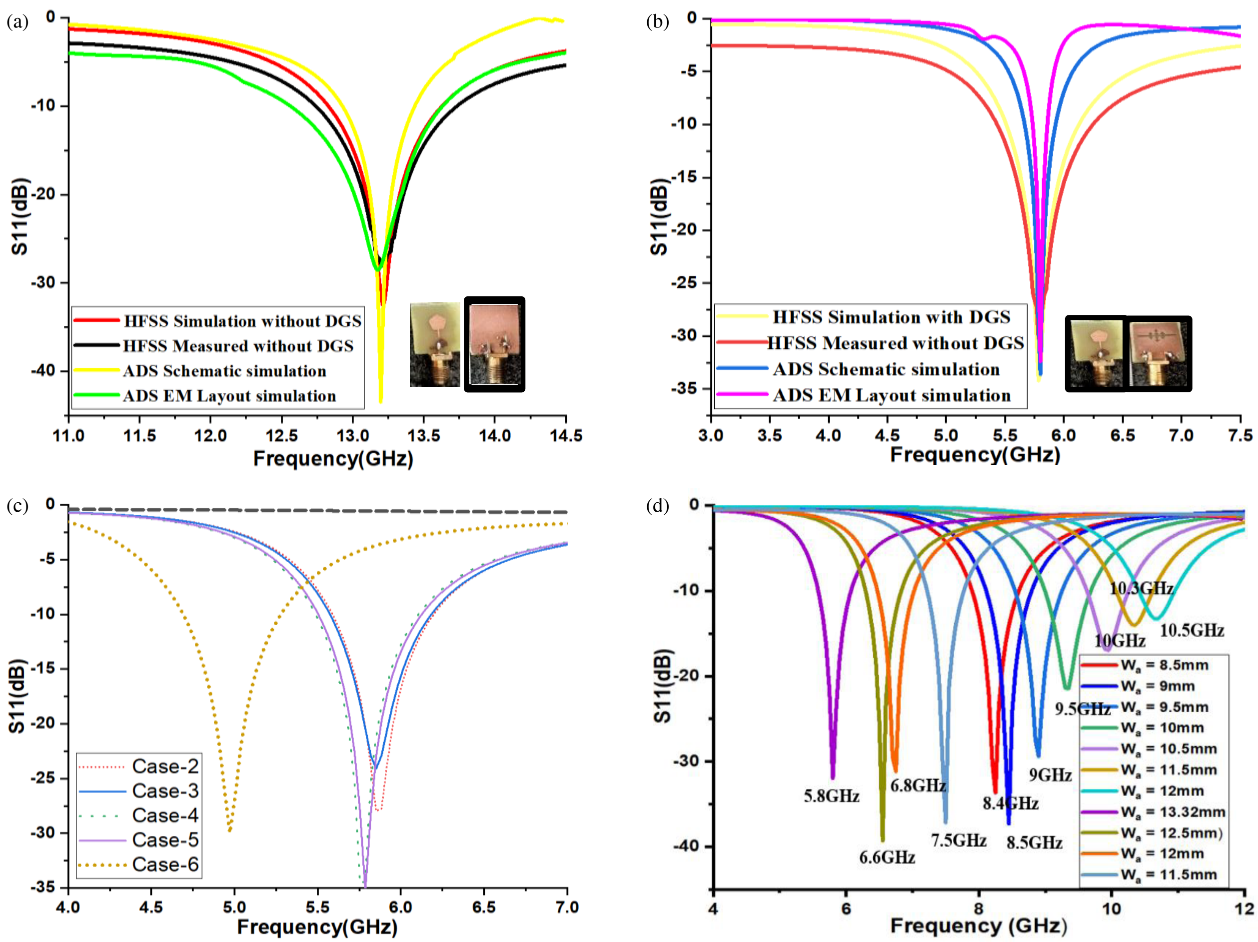

FIGURE 5. Comparison of S_{11} with frequency: (a) simulated single-band patch with HFSS, circuit layout, and electromagnetic schematic simulation with ADS, (b) measured results, (c) simulation technique utilised in the development of a single-band antenna, and (d) simulation of KCF-DGS with (iteration 0) utilising an alternative size 'W_0' of slot.

KCF-DGS, the size of the rectangular slot fluctuates by 0.5 mm in iteration 0. This facilitates the initial resonant frequencies (from right toward left) to transition to a smaller frequency.

Figure 6(a) illustrates the 3D gain plot and current dispersion along the length of the feed line at 13.2 GHz within the Ku band. Figure 6(b) depicts the relationship involving the margin currents of the iterated KCF-DGS fractal and patch at

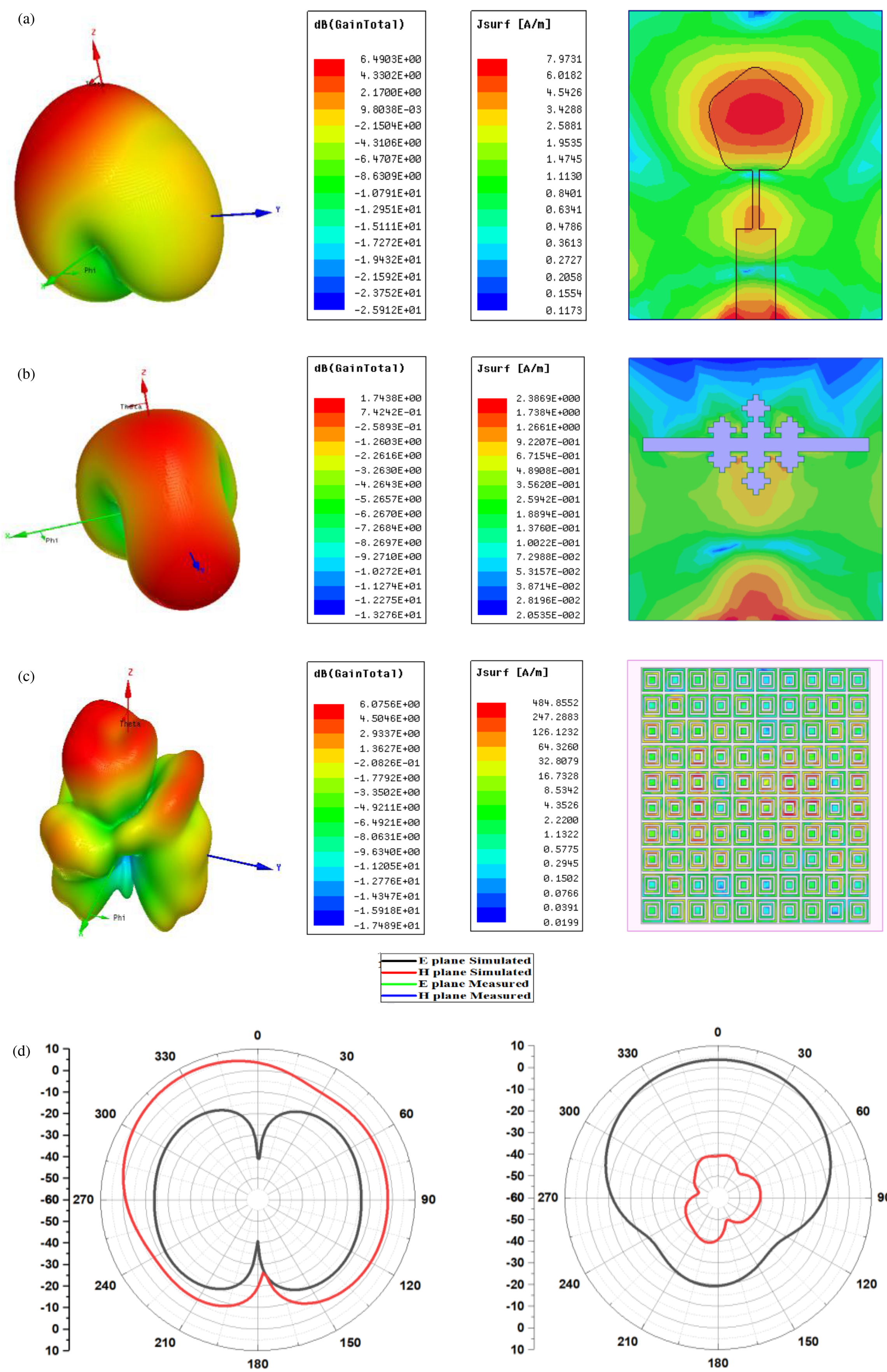
(a)
dB(GainTotal)
6.4903E+00
4.3302E+00
2.1700E+00
9.8038E-03
-2.1504E+00
-4.3106E+00
-6.4707E+00
-8.6309E+00
-1.0791E+01
-1.2951E+01
-1.5111E+01
-1.7272E+01
-1.9432E+01
-2.1592E+01
-2.3752E+01
-2.5912E+01
Jsurf [A/m]
7.9731
6.0182
4.5426
3.4288
2.5881
1.9535
1.4745
1.1130
0.8401
0.6341
0.4786
0.3613
0.2727
0.2058
0.1554
0.1173
(b)
dB(GainTotal)
1.7438E+00
7.4242E-01
-2.5893E-01
-1.2603E+00
-2.2616E+00
-3.2630E+00
-4.2643E+00
-5.2657E+00
-6.2670E+00
-7.2684E+00
-8.2697E+00
-9.2710E+00
-1.0272E+01
-1.1274E+01
-1.2275E+01
-1.3276E+01
Jsurf [A/m]
2.3869E+000
1.7384E+000
1.2661E+000
9.2207E-001
6.7154E-001
4.8908E-001
3.5620E-001
2.5942E-001
1.8894E-001
1.3760E-001
1.0022E-001
7.2988E-002
5.3157E-002
3.8714E-002
2.8196E-002
2.0535E-002
(c)
dB(GainTotal)
6.0756E+00
4.5046E+00
2.9337E+00
1.3627E+00
-2.0826E-01
-1.7792E+00
-3.3502E+00
-4.9211E+00
-6.4921E+00
-8.0631E+00
-9.6340E+00
-1.1205E+01
-1.2776E+01
-1.4347E+01
-1.5918E+01
-1.7489E+01
Jsurf [A/m]
484.8552
247.2883
126.1232
64.3260
32.8079
16.7328
8.5342
4.3526
2.2200
1.1322
0.5775
0.2945
0.1502
0.0766
0.0391
0.0199
E plane Simulated
H plane Simulated
E plane Measured
H plane Measured
(d)

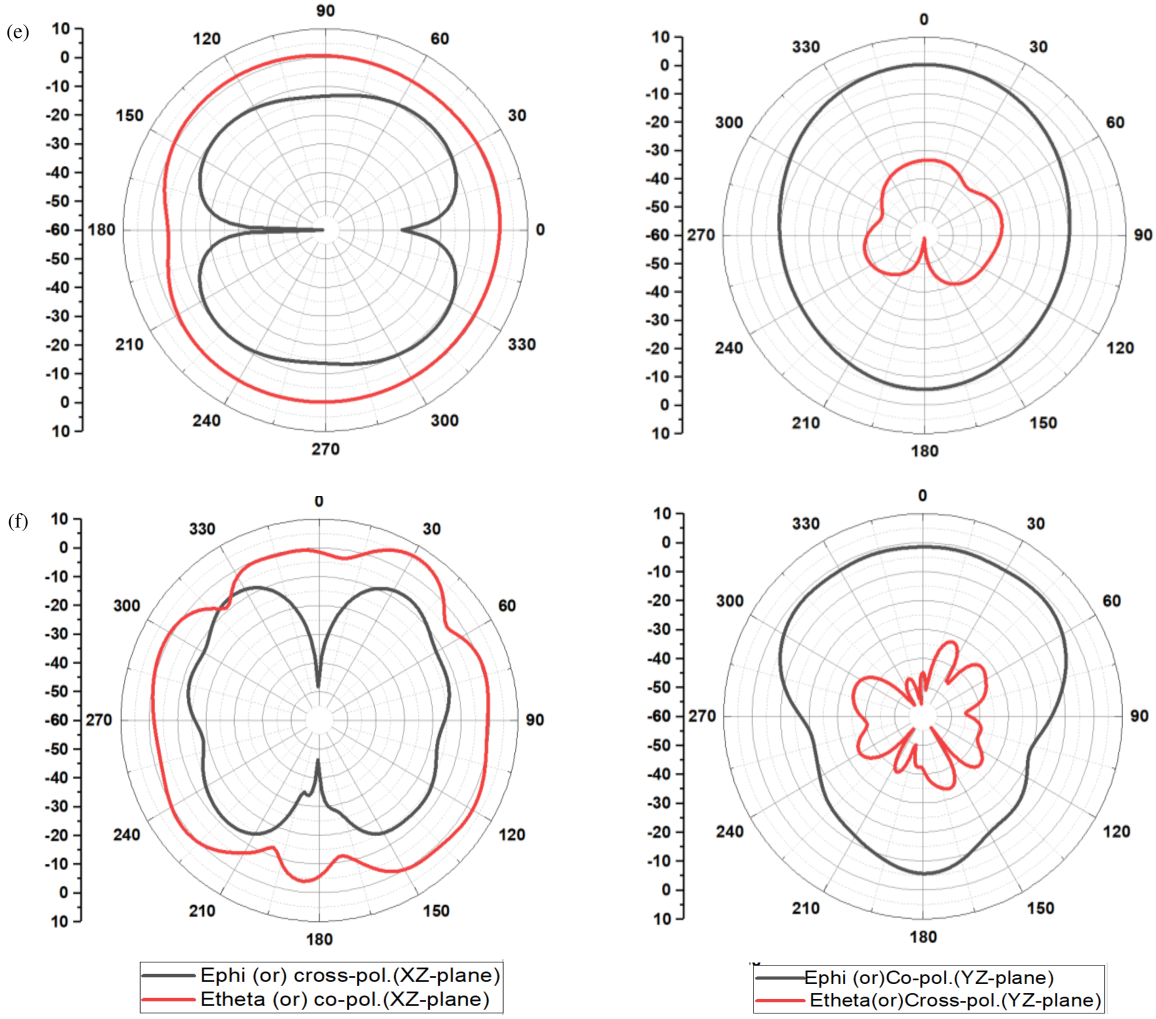

FIGURE 6. 3D gain plot and current distribution (a) for conventional antenna at 13.2 GHz, (b) with DGS, (c) with DGS and FSS, and measured, simulated radiation pattern results, (d) for the conventional antenna at 13.2 GHz, (e) with DGS 5.8 GHz, and (f) with DGS and FSS at 5.8 GHz for miniaturized antenna.

5.8 GHz within the C band. Figure 6(c) shows the current distributions of the KCF-DGS fractal and FSS at 5.8 GHz in the C band. Figures 6(d), (e), and (f) illustrate the simulated and measured radiation patterns of the proposed antenna in the E-plane and H-plane. The E-plane radiation pattern exhibits a bidirectional characteristic with pronounced maxima near 90° and 270° and nulls around 0° and 180°. In contrast, the H-plane demonstrates a nearly omnidirectional radiation characteristic with relatively uniform radiation intensity over the azimuth plane. In the XZ-plane, the co-polarized component ($E\theta$) dominates the radiation characteristics, while the cross-polarized component ($E\varphi$) remains significantly lower over most angular regions. The radiation pattern exhibits a bidirectional characteristic with pronounced nulls near 0° and 180°. In the YZ-plane, the antenna produces a broadside radiation pattern with the main lobe directed normal to the antenna surface. The cross-polarization levels are substantially suppressed compared to the co-polarized fields, demonstrating good polarization purity. Furthermore, the radiation patterns remain largely unchanged across the operating frequencies, indicating stable radiation behavior and consistent antenna performance throughout the operating bandwidth. The measured and simulated results show good agreement, validating the effectiveness of the proposed design. The maximum gain associated with the single-band patch antenna is observed at a Ku-band frequency of 13.2 GHz, as illustrated in Figure 7(a). The measured peak directivity and peak gain of a loaded KCF-DGS traditional antenna and FSS at 5.8 GHz are shown in Figure 7(b) as 1.74 to 7.40 dBi and 3.53 to 7.95 dBi, respectively. In a traditional time-domain investigation, the fidelity factor is an essential component that reveals the antenna's characteristics. To reduce losses in the signal modulated in electronic communication, there is a strong connection between the sending and receiving signals. To evaluate the pulse measurement attributes of the suggested antenna reduction, Figure 7(c) shows two similar antennas placed adjacent to one another, 40 cm apart. Figures 7(d), (e), and (f) delineate the simulated and experimental characteristics of received and input signals in a time-domain methodology. The fidelity factor correlation is computed [25], and the resemblance of the received and input signals is deter-

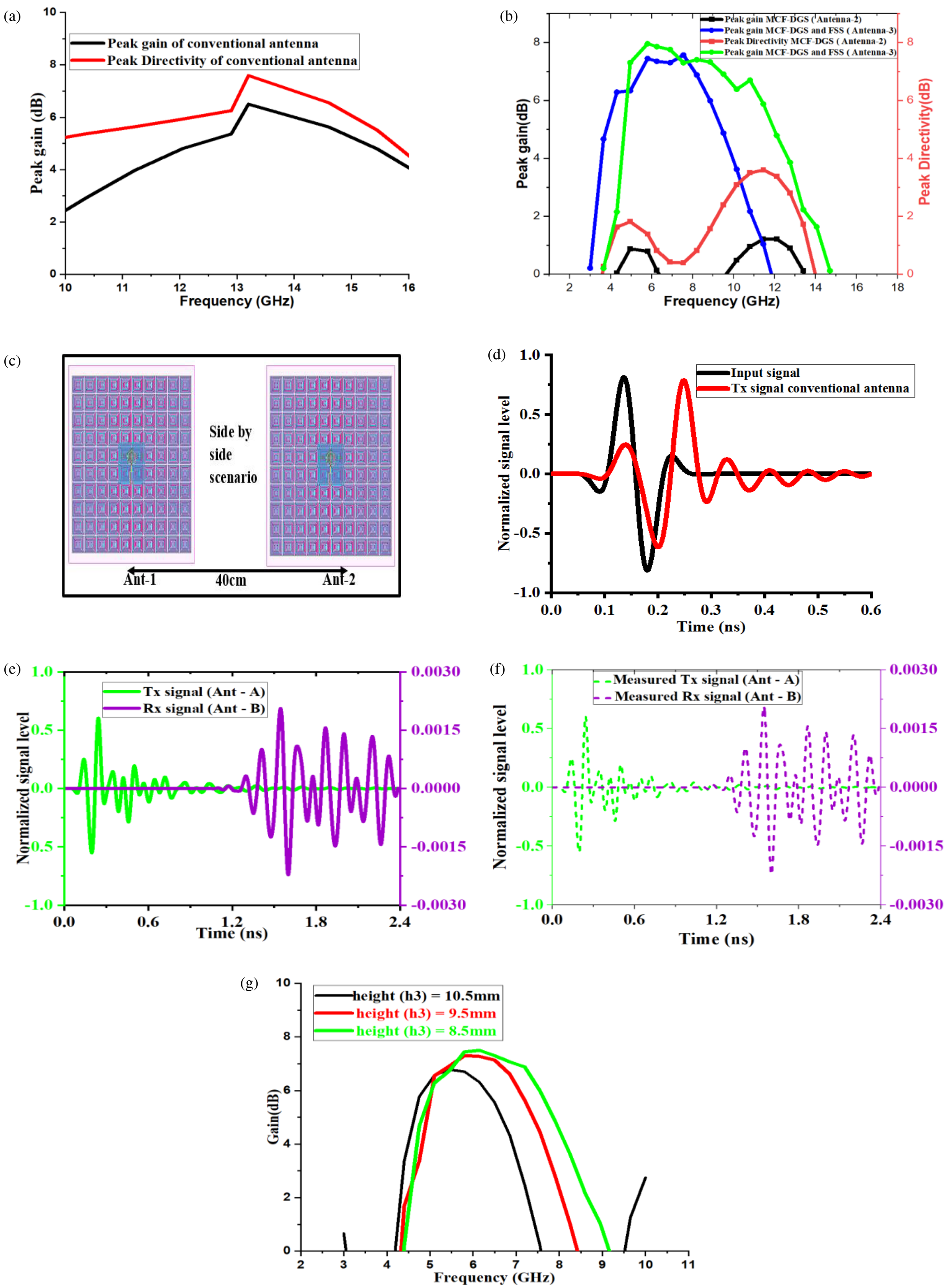

FIGURE 7. Results of measured peak directivity and peak gain vs frequency for (a) patch antenna, (b) single working band antenna, (c) concurrent scenario for time-varying achievement, (d) the normalised signal level — input and transmitted signal, (e) simulated, transmitted and received signals, (f) measured transmitted and received signals, and (g) patch with different heights of placing FSS.

TABLE 5. Performance comparison of the proposed antenna with previously reported miniaturized antennas.

Ref	size (mm^2)	Resonance Switching Frequency [GHz]		Type of loading	Miniaturization (%)	working bands	Gain (dBi)	Fidelity factor
		Before switch	After switch					
[2]	$0.561\lambda * 0.561\lambda$	2.01	1.53	Loop	23.88	Single	-3.4	No
[3]	$0.812\lambda * 0.812\lambda$	3.26	2.03	Wire	28.83	Single	NA	No
[4]	$1.16\lambda * 1.16\lambda$	3.26	2.32	Slit, strip	37.73	Single	0.5 dB	No
[13]	$0.3\lambda * 0.3\lambda$	4.2	2.5	Fractal EBG and SRR	40.47	Single	3.77	No
[14]	$0.5\lambda * 0.5\lambda$	4.225	2.5	HRI metamaterial	40.8	Single	-1.1	No
Proposed	$0.26\lambda * 0.31\lambda$	13.2	5.8	MCF-DGS	56	Single	7.32	Yes

mined using Eq. (17). $x(t)$ signifies the sent signal, whereas $y(t)$ represents the incoming signal. For the data being entered and transferred signal, the obtained fidelity factor is 84% between the input and transmitted signals, 80% between the transmitted and received signals, and 78% for the experimentally measured transmitted and received signal.

Figure 7(g) represents the patch with different heights of placing FSS. Table 5 compares previously published findings with the suggested miniaturized single-band antenna.

$$F = \max_{\tau} \left| \frac{\int_{-\infty}^{+\infty} a(t)\, b(t-\tau)\, dt}{\sqrt{\int_{-\infty}^{+\infty} a(t)^2 dt \int_{-\infty}^{+\infty} b(t)^2 dt}} \right| \tag{17}$$

4. CONCLUSION

This article presents a miniaturized Pentagonal Antenna (MPA)-loaded Minkowski Curve, Fractal Defected Ground Structure (MCF-DGS) with Frequency Selective Surface (FSS) for 5.725–5.875 GHz WLAN applications, which operates at 5.8 GHz, has S_{11} of -32.45 dB, respectively, and achieves a miniaturization of 56%. The antenna is $15 \times 16 \times 1.6\,\mathrm{mm}^3$ (or) $0.29\lambda_0 \times 0.30\lambda_0\,\mathrm{mm}^2$ in size, based on an FR4 epoxy with a peak directivity of 7.95 dBi. It functions in single band. An MCF-DGS achieves Ka ≤ 1 at 5.8 GHz. To ascertain the fidelity factor of the proposed antenna, a time-domain analysis was performed in a side-to-side arrangement. In terms of percentages, the 0.80 GHz bandwidth was 3.46 percent.

REFERENCES

[1] Fallahpour, M. and R. Zoughi, "Antenna miniaturization techniques: A review of topology-and material-based methods," *IEEE Antennas and Propagation Magazine*, Vol. 60, No. 1, 38–50, Feb. 2018.

[2] Chu, L. J., "Physical limitations of omnidirectional antennas," *J. Applied Physics*, Vol. 19, 1163–1175, Dec. 1948.

[3] Ghosh, B., S. K. M. Haque, and N. R. Yenduri, "Miniaturization of slot antennas using wire loading," *IEEE Antennas and Wireless Propagation Letters*, Vol. 12, 488–491, 2013.

[4] Erentok, A. and R. W. Ziolkowski, "Metamaterial-inspired efficient electrically small antennas," *IEEE Transactions on Antennas and Propagation*, Vol. 56, No. 3, 691–707, Mar. 2008.

[5] Jahani, S., M. J. Rashed, and M. Shahabadi, "Miniaturization of circular patch antennas using MNG metamaterials," *IEEE Transactions on Antennas and Propagation*, Vol. 9, No. 5, 1194–1196, Dec. 2010.

[6] Erentok, A. and R. W. Ziolkowski, "Metamaterial-inspired efficient electrically small antennas," *IEEE Transactions on Antennas and Propagation*, Vol. 56, No. 3, 691–707, Mar. 2008.

[7] Wheeler, H. A., "Fundamental limitations of small antennas," *Proceedings of the IRE*, Vol. 35, No. 12, 1479–1484, Dec. 1947.

[8] Chu, L. J., "Physical limitations of omni-directional antennas," *Journal of Applied Physics*, Vol. 19, No. 12, 1163–1175, Dec. 1948.

[9] Haque, S. M. and K. M. Parvez, "Slot antenna miniaturization using slit, strip, and loop loading techniques," *IEEE Transactions on Antennas and Propagation*, Vol. 65, No. 5, 2215–2221, May 2017.

[10] Jahani, S., J. Rashed-Mohassel, and M. Shahabadi, "Miniaturization of circular patch antennas using MNG metamaterials," *IEEE Antennas and Wireless Propagation Letters*, Vol. 9, 1194–1196, 2010.

[11] Khan, M. U., M. S. Sharawi, and R. Mittra, "Microstrip patch antenna miniaturisation techniques: A review," *IET Microwaves, Antennas & Propagation*, Vol. 9, No. 9, 913–922, 2015.

[12] Shrestha, S., S. R. Lee, and D.-Y. Choi, "A new fractal-based miniaturized dual band patch antenna for RF energy harvesting," *International Journal of Antennas and Propagation*, Vol. 2014, No. 1, 805052, 2014.

[13] Mishra, N. and R. K. Chaudhary, "A miniaturised directive high gain metamaterial antenna using ELC ground for WiMAX application," *International Journal of Electronics Letters*, Vol. 7, No. 1, 68–76, 2019.

[14] Reddy, G. B., M. H. Adhithya, and D. S. Kumar, "Miniaturization of microstrip slot antenna using high refractive index metamaterial based on single ring split ring resonator," *Progress In Electromagnetics Research Letters*, Vol. 93, 115–122, 2020.

[15] Sharma, N. and V. Sharma, "A design of microstrip patch antenna using hybrid fractal slot for wideband applications," *Ain Shams Engineering Journal*, Vol. 9, No. 4, 2491–2497, 2018.

[16] Ao, J., J. Huang, W. Wu, and N. Yuan, "A miniaturized vivaldi antenna by loading with parasitic patch and lumped resistor," *AEU — International Journal of Electronics and Communications*, Vol. 81, 158–162, 2017.

[17] Er-Rebyiy, R., J. Zbitou, M. Latrach, A. Tajmouati, A. Errkik, and L. E. Abdellaoui, "New miniature planar microstrip antenna using DGS for ISM applications," *TELKOMNIKA (Telecommunication Computing Electronics and Control)*, Vol. 15, No. 3, 1149–1154, 2017.

[18] Oulhaj, O., N. A. Touhami, M. Aghoutane, and A. Tazón, "A miniature microstrip patch antenna array with defected ground structure," *International Journal of Microwave and Optical Technology (IJMOT)*, Vol. 11, No. 1, 32–39, 2016.

[19] Hanae, E., N. A. Touhami, and M. Aghoutane, "Miniaturized microstrip patch antenna with spiral defected microstrip structure," *Progress In Electromagnetics Research Letters*, Vol. 53, 37–44, 2015.

[20] Elftouh, H., N. A. Touhami, M. Aghoutane, S. E. Amrani, A. Tazón, and M. Boussouis, "Miniaturized microstrip patch antenna with defected ground structure," *Progress In Electromagnetics Research C*, Vol. 55, 25–33, 2014.

[21] Ghaloua, A., J. Zbitou, L. E. Abdellaoui, M. Latrach, A. Tajmouati, and A. Errkik, "A novel configuration of a miniature printed antenna array based on defected ground structure," *International Journal of Intelligent Engineering and Systems*, Vol. 12, No. 1, 211–220, 2019.

[22] Carver, K. and J. Mink, "Microstrip antenna technology," *IEEE Transactions on Antennas and Propagation*, Vol. 29, No. 1, 2–24, 1981.

[23] Volakis, J. L., C.-C. Chen, and K. Fujimoto, *Small Antennas: Miniaturization Techniques and Applications*, McGraw-Hill, 2010.

[24] Hansen, R. C. and R. E. Collin, *Small Antenna Handbook*, John Wiley & Sons, 2011.

[25] Quintero, G., J.-F. Zurcher, and A. K. Skrivervik, "System fidelity factor: A new method for comparing UWB antennas," *IEEE Transactions on Antennas and Propagation*, Vol. 59, No. 7, 2502–2512, 2011.

[26] Langley, R. J. and E. A. Parker, "Equivalent circuit model for arrays of square loops," *Electronics Letters*, Vol. 18, No. 7, 294–296, 1982.